Progress In Electromagnetics Research M, Vol. 114, 49–57, 2022

A Comparison of Two Generalizations to the Linear Sampling Method for Inverse Scattering

Yeasmin Sultana and James E. Richie*

Abstract—The linear sampling method (LSM) is a very popular method for determining the boundary of an object from the scattered field. However, there are instances where LSM provides the convex hull of the boundary rather than the true boundary. There are two common generalizations to LSM: the Generalized Linear Sampling Method (GLSM) and the Multipoles-based Linear Sampling Method (MLSM). In this paper, the ability of GLSM and MLSM to overcome some of the deficiencies of LSM are investigated. It is found that GLSM may be ideal for imaging thin features of scatterers and that MLSM can provide an improvement over LSM in a more general sense. GLSM may also require user input to adjust the indicator function whereas MLSM does not appear to rely as much on indicator function adjustments for adequate results.

1. INTRODUCTION

Techniques in inverse scattering use the measured scattered field to estimate the boundary and composition of unknown objects. Approaches that solve the full problem (both the boundary and composition) are denoted quantitative approaches whereas methods that estimate only some of the object's characteristics are called qualitative methods.

There are many applications of inverse scattering methods, both quantitative and qualitative. Several areas of application are described in [1]. Quantitative methods have been applied to food quality [2], breast imaging [3], brain stroke detection [4], and subsurface prospecting [5]. Recently, quantitative inverse scattering methods have been applied to antenna design as well [6]. Qualitative method applications include breast imaging [7] and ground penetrating radar [8].

The computational burden of the qualitative problem is often much smaller than solving the full quantitative problem. Some qualitative methods have a common trait: they estimate the boundary of the object by sampling the domain and use an indicator function to predict whether each sample point is inside or outside the scatterer. An early technique is the Linear Sampling Method (LSM) [9]. There are other methods in this category, including the Multipoles-based Linear Sampling Method (MLSM) [10] and a Generalized LSM (GLSM) [11]. In most of these methods, a linear ill-posed problem is solved at each sample point. A more recently reported method, the orthogonal sampling method (OSM) [12] and its near-field extension (NF-OSM) [13] are qualitative methods that are very different from the LSM family of methods.

These qualitative methods are not iterative and therefore usually do not adequately solve the problem. The sampling methods are also more susceptible to noise. Taken together, these shortcomings mean that determination of the boundary may be difficult [14]. However, the information obtained from the sampling methods can still be useful, for example to limit the support domain of the scatterer in a quantitative procedure.

Received 18 August 2022, Accepted 14 October 2022, Scheduled 17 October 2022
* Corresponding author: James E. Richie (james.richie@marquette.edu).
The authors are with the Electrical and Computer Engineering Department, Marquette University, USA.

In [15], the performance of three qualitative methods are compared: The LSM, the OSM, and Boundary retrieval through Inverse source and Sparsity (B-IS) [16]. In this work, results using LSM, GLSM, and MLSM will be compared. Both GLSM and MLSM are closely related to the original LSM method; however, each technique attempts to improve the effectiveness of LSM when determining the boundary of an object. Each method will be described and used to image synthetic data from scatterers.

There are several different methods for computing the scattered data. One method uses the moment method [17]. More recently, other numerical techniques have been developed. The MEEP software [18] is a finite-difference time-domain solver that is very versatile. In this work, all field computations are done using MEEP.

2. THE LINEAR SAMPLING METHOD AND ITS GENERALIZATIONS

A typical inverse scattering scenario is shown in Fig. 1. The measurements can be over many scattered directions with multiple incident field directions. In addition, the scattered field data can be at a single frequency or consist of multi-frequency measurements. In this work, there is a collection of antennas surrounding the unknown object. The object is inside some background permittivity, ϵ_b (here, free space is assumed). For each experiment, one antenna transmits a fixed frequency signal in the $\vec{k}$ direction with TM^z polarization and the field is measured at M locations, denoted as $\vec{r}_m$. The angle of incidence is denoted as ϕ_n^i. There are N experiments corresponding to N incident field directions. The result is a matrix of scattered electric field values, $E^s(\vec{r}_m, \phi_n^i)$ where each column of the matrix corresponds to one experiment. An $\exp\{j\omega t\}$ time dependence is assumed throughout.

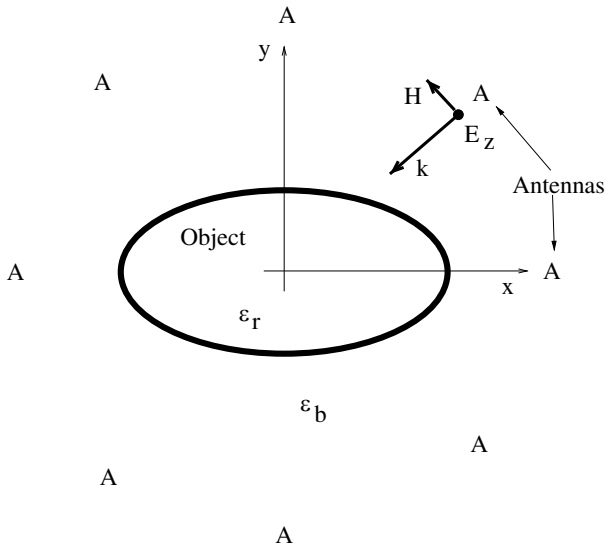

Figure 1. Geometry for the data collection. Each 'A' represents a transmit or receive antenna.

2.1. The Linear Sampling Method

The linear sampling method (LSM) [9, 19, 20] is a qualitative approach to inverse scattering. LSM can estimate the boundary of an unknown object by choosing a grid of sample points ($\vec{r}_p$) within the object domain and computing an indicator value for each sample point. The indicator is used to decide whether each sample point on the grid is inside or outside the object.

In LSM, a linear combination of experiments is sought that results in a *scattered field* that is *focused* [20] around the sample point. The norm of the vector that describes the linear combination is the basis for the indicator. Mathematically,

$$\sum_{n=1}^{N} \xi_n(\vec{r}_p) E^s(\vec{r}_m, \phi_n^i) = G_o(\vec{r}_m, \vec{r}_p) \tag{1}$$

where $G_o(\vec{r}_m, \vec{r}_p)$ is the Green's function describing the radiation observed at $\vec{r}_m$ due to a point source located at $\vec{r}_p$:

$$G_o(\vec{r}_m, \vec{r}_p) = H_o^{(2)}(k_b|\vec{r}_m - \vec{r}_p|) \tag{2}$$

where k_b is the wavenumber for the background material, and $H_o^{(2)}$ is the Hankel function of the second kind of order zero, representing outgoing waves. The vector ξ_n represents the linear combination of experiments that results in a scattered field at all $\vec{r}_m$ that matches the field of a point source at $\vec{r}_p$.

Equation (1) is generally ill-posed; therefore, some regularization must be applied to determine the vector ξ_n. LSM as implemented in [20] uses the singular value decomposition (SVD) on E^s. Consider the matrix equation for a single $\vec{r}_p$:

$$E^s\xi = G_o \tag{3}$$

where E^s is an $M \times N$ matrix; ξ is a vector of length N; and G_o is a vector of length M. Apply SVD

$$E^s = VSU^H \rightarrow \xi = V^H S^{-1} U G_o \tag{4}$$

where S is a diagonal matrix of the singular values s_{nn}. To regularize the solution, replace the S^{-1} entries with

$$\frac{s_{nn}}{s_{nn}^2 + \alpha^2} \tag{5}$$

where α is the regularization parameter, chosen as $\alpha = 0.01 s_{11}$. Note that the SVD step is performed once on the scattered field matrix. The same SVD solution is used for each $\vec{r}_p$ in the domain.

The entries of the vector ξ also have a physical interpretation related to the concept of 'virtual experiments' [21]. The values correspond to the amplitude and phase of the excitation at each of the N transmit locations. The linear combination of experiments with ξ as weights produces a scattered field that replicates the field at the observation locations of a point source situated at $\vec{r}_p$. In general, the scattered field is focused near $\vec{r}_p$ and is typically circularly symmetric about $\vec{r}_p$.

To illustrate some of these ideas, a data matrix is computed using MEEP [18] for a scatterer with elliptical cross section (major axis $a = 0.5\lambda_b$, minor axis $b = 0.25\lambda_b$) with $\epsilon_r = 2.0$. Eq. (1) is solved for a sample point at the origin (within the object). A virtual experiment is simulated via MEEP using the ξ vector obtained. The total field for the virtual experiment is shown in Fig. 2(a) and the scattered field is shown in Fig. 2(b). The location of the transmitters are on a circle of radius $2\lambda_b$. Some transmitter locations can be seen in Fig. 2(a). Fig. 2(b) clearly shows that the scattered field is roughly circular near the receiver locations (which are identical to the transmitter locations).

The vector ξ is used to determine whether the point $\vec{r}_p$ is inside or outside the object by using an indicator function. The norm of $\xi_n(\vec{r}_p)$ (see Eq. (1)) is used as the indicator function. Small values

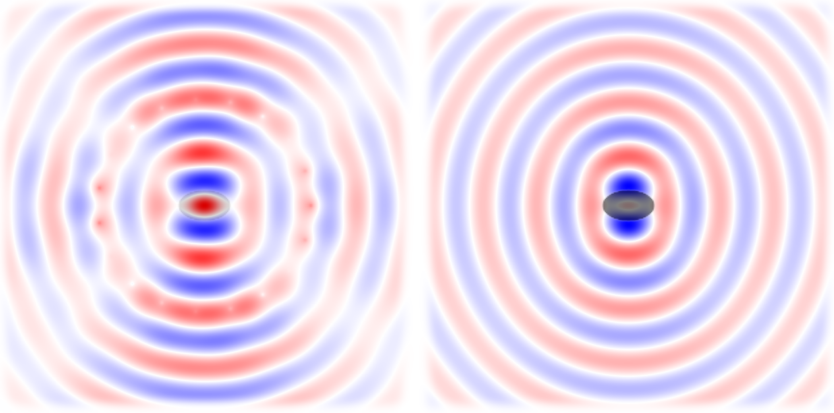

(a) (b)

Figure 2. Virtual experiment fields with $\vec{r}_p$ at origin. Scatterer has an elliptical cross section: (a) total field; (b) scattered field with scatterer shown in gray.

of $\|\xi\|^2$ are considered to be inside the object and large values are outside the object. Specifically, the indicator function used with LSM is

$$I_{LSM} = -\log_{10} \frac{\|\xi\|^2}{\|\xi\|^2_{\max}} \tag{6}$$

where it is noted that small values for $\|\xi\|^2$ correspond to $\vec{r}_p$ within the object and result in large positive I_{LSM}. To distinguish between 'inside' and 'outside', a suitable threshold is chosen. For example, $\vec{r}_p$ is inside the object if $I_{LSM} > \delta\ I_{LSM,\max}$ where $0 < \delta < 1$. The choice of δ is often heuristic and becomes more difficult in the presence of noise [14]. In this work, the choice for δ will be analyzed for a number of scenarios in LSM, GLSM, and MLSM.

The LSM method is very versatile and popular; however, there are object shapes that LSM may give a boundary that is not the true shape of the scatterer [11]. It is for this reason that the GLSM and MLSM techniques have been developed.

2.2. The Generalized Linear Sampling Method [11]

In GLSM, (1) is modified to:

$$\sum_{n=1}^{N} \xi^{e,o}_{\ell,n}(\vec{r}_p) E^s(\vec{r}_m, \phi^i_n) = G^{e,o}_\ell(\vec{r}_m, \vec{r}_p) \tag{7}$$

where the right hand side is now an even/odd *multipole* of order ℓ:

$$G^{e,o}_\ell(\vec{r}_m, \vec{r}_p) = H^{(2)}_\ell(k_b|\vec{r}_m - \vec{r}_p|)^{\cos}_{\sin}(\ell\phi) \tag{8}$$

where the even (e) version corresponds to the upper (cos) term, and the odd version corresponds to the lower (sin) term.

Switching from a monopole to a multipole introduces additional considerations. Scattering from a very small object typically results in a monopole scattered field. For a multipole, the object must have dimensions large enough to support multipole radiation. For a source within a ball of radius a, the largest multipole order that can be supported is on the order of $n = k_b a$.

Denote the ball of radius a as the support ball. There are two implications of the support ball. First, using a multipole in GLSM means that the sample point can not be too close to the edge of the object (or insufficient support is present). Second, sample points in thin objects or objects with thin features may not be capable of supporting some multipole configurations.

In many cases, the LSM monopole is sufficient. LSM uses test points and determines if a singularity can be created at the test point using the scattered field data. For convex object boundaries, this works well. Define the convex hull of the object boundary as the smallest convex shape that encloses the boundary. Where the object boundary has a concave portion, points between the object boundary and the convex hull can support zero order singularities as a consequence of the equivalence principle. This is formally demonstrated in Appendix B of [11] for an annulus; however, a partial annulus could be considered as an approximation to the concave section of an object. Therefore, the use of multipoles may be helpful in finding a more accurate object shape even for objects with a convex hull significantly different from the object boundary.

Using higher order poles in GLSM can help identify regions that are hollow or concave by choosing an appropriate indicator function. In [11], the indicator is defined as

$$I_{GLSM} = -\log_{10} \frac{\Xi_P}{\Xi_{P,\max}} \tag{9}$$

where

$$\Xi_P = \prod_{\ell=1}^{P} \frac{\|\xi\|^2}{\|\xi^e_\ell\|^2} \frac{\|\xi\|^2}{\|\xi^o_\ell\|^2} \tag{10}$$

$\|\xi^{e,o}_\ell\|^2$ is the norm of the vector found in (7), and $\|\xi\|^2$ is the norm of the LSM result. The form of I_{GLSM} is similar to I_{LSM} in (6). A similar, suitable threshold (δ) for I_{GLSM} is chosen to distinguish

between 'inside' and 'outside'. Consider a thin scatterer with a cross section that is mostly parallel to the y axis. A y-directed dipole can be supported by the scatterer and ξ_1^o would have a small norm for some sample points. The indicator function would then correctly interpret $\vec{r}_p$ as inside the object.

The concept of virtual experiments can be applied to the generalized case as well. Fig. 3(a) shows the total field of a virtual experiment derived from $\xi_1^e(\vec{r}_p)$ with $\vec{r}_p$ at the origin. Fig. 3(b) shows the corresponding scattered field. Results were obtained using MEEP. The object is the same elliptical scatterer that was used for Fig. 2. In Fig. 3, one can see the ϕ variation due to the use of a higher order pole in GLSM.

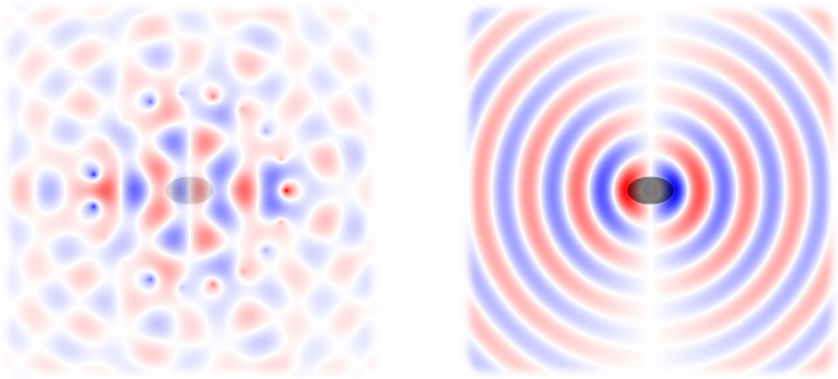

(a) (b)

Figure 3. Virtual experiment fields for elliptical scatterer using even dipole in GLSM. $\vec{r}_p$ is at the origin: (a) total field; (b) scattered field, with object shown in gray.

2.3. The Multipoles-Based Linear Sampling Method [10]

In MLSM, the far-field data is expanded in a multipole expansion about the sample point. The expansion is truncated to perform regularization. The expansion coefficients are then used to find a linear combination of experiments that results in a large monopole contribution while the other poles kept in the expansion are forced to combine to zero field.

Mathematically, the first step is written as:

$$E^s(\vec{r}_m, \phi_n^i) = \sum_{\ell=-L}^{L} \alpha_\ell(\vec{r}_p, \phi_n^i) H_\ell^{(2)}(k_b|\vec{r}_m - \vec{r}_p|) e^{j\ell Arg(\vec{r}_m - \vec{r}_p)} \tag{11}$$

The $E^s(\vec{r}_m, \phi_n^i)$ term is the measured data, and the $H_\ell^{(2)}(k_b|\vec{r}_m - \vec{r}_p|)e^{j\ell Arg(\vec{r}_m - \vec{r}_p)}$ term is cast as a matrix to solve for the unknown multipole expansion coefficients, α_ℓ. There are $2L+1$ coefficients for each of N experiments. A pseudo-inverse solution to find α_ℓ is recommended in [10]. The series is truncated at L to perform regularization. Often, L is chosen to be 1 so that only the monopole and the two dipole terms are kept in the expansion. This has been observed to be sufficient in most cases. A small L also keeps the computation time per sample point smaller [10]. In this work, $L = 1$ is sufficient to obtain satisfactory results in all cases. However, we have observed that larger objects may require larger L to obtain similar accuracy.

The second step consists of combining the expansions in a linear combination that preserves the monopole but extinguishes the higher order pole contributions:

$$Ah = D \tag{12}$$

where A is the $(2L+1) \times N$ matrix of multipole coefficients α_ℓ; h is the unknown linear combination of N experiments; and D is a known vector with $2L+1$ entries all of which are zero except the center element is one.

The concept of virtual experiments can be applied to the multipoles-based case as well. Fig. 4 shows virtual experiment results using MEEP and the h vector found using $L = 1$ and $\vec{r}_p$ at the origin

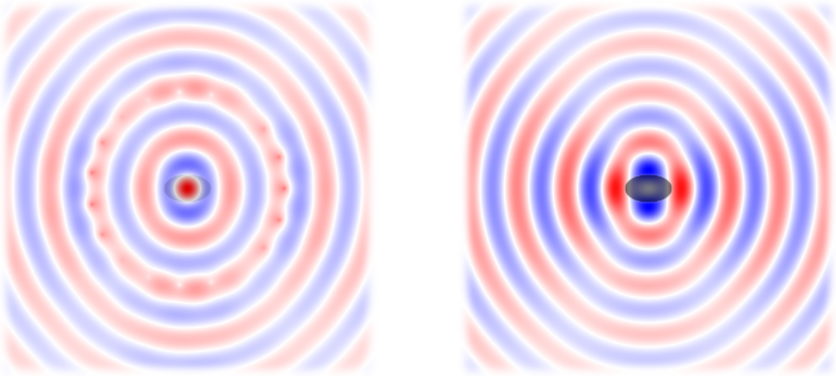

(a) (b)

Figure 4. Virtual experiment fields with $\vec{r}_p$ at origin: (a) total field; (b) scattered field with scatterer in gray.

in MLSM. The scatterer is the same as the virtual experiment results in Figs. 2 and 3. Fig. 4 is similar to Fig. 2. In each case, the virtual experiment should result in the fields of a monopole located at the origin. However, in Fig. 2, LSM is used and in Fig. 4 the data is pre-conditioned by computing a truncated multipole expansion. The ϕ symmetry is not as precise in the MLSM case, as seen in Fig. 4(b).

The indicator function is very similar to the LSM case:

$$I_{MLSM} = -\log_{10} \frac{\|h\|^2}{\|h\|^2_{\max}} \tag{13}$$

and it has the same characteristics as the other indicators discussed previously. In [10], it is suggested that the indicator function be interpreted where $\vec{r}_p$ is within the object if I_{MLSM} is within $\delta = 0.8$ of the maximum.

In LSM and GLSM, regularization occurs in the SVD calculation, where the singular values are adjusted using a regularization parameter, α. The SVD is computed once and used for every sample point $\vec{r}_p$. In MLSM, the data is regularized by truncating the multipole expansion of the data relative to the sample point. However, in MLSM a multipole expansion is computed for every sample point $\vec{r}_p$.

3. SIMULATION RESULTS

In this section, simulation will be used to create synthetic data and to demonstrate some of the results from the previous section. Each data matrix is computed using MEEP [18], an open-source, finite-difference time-domain electromagnetic solver.

The first scatterer has a simple elliptical cross section, with major axis $a = 0.5\lambda$ and minor axis $b = 0.25\lambda$. The relative permittivity (ϵ_r) is 2.0. This is the scatterer used to simulate the virtual experiments of Figs. 2, 3, and 4. The results are summarized in Fig. 5. Each graphic in Fig. 5 shows indicator function data on a gray scale and the outline of the scatterer. Also shown is the approximate boundary found using each method. The LSM results (Fig. 5(a)) for the elliptical scatterer are very good. MLSM (Fig. 5(b)) appears to estimate the object slightly larger along with GLSM when $P = 2$ (Fig. 5(c)). The GLSM, $P = 3$ case (Fig. 5(d)) appears to be very good except for the spatial oscillations in the estimated boundary (which also appear in the $P = 2$ case).

Results for an S-shaped scatterer with $\epsilon_r = 2.0$ are shown in Fig. 6, using the same format as Fig. 5. In the S-shaped scatterer, LSM has difficulty determining the shape accurately, as may be expected from the non-convex features. The MLSM reconstruction is very good, but neither GLSM case images the interior vertical section. Note again the estimated boundary oscillations in the GLSM case.

Figure 7 shows the results for a thin U shaped target and a similar but thicker U shaped target. The thin target is not well-reconstructed in the case of MLSM (Fig. 7(a)); however, GLSM appears to

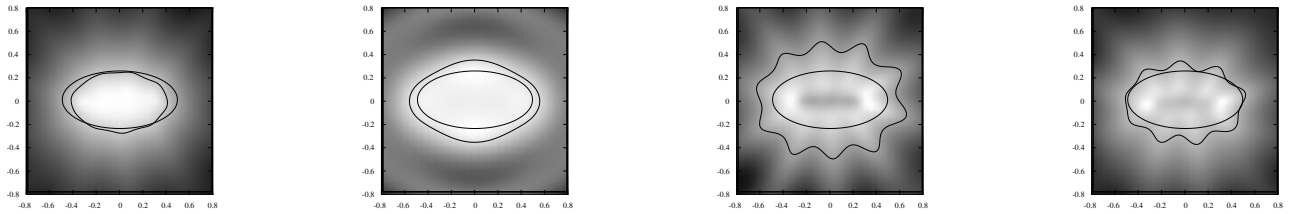

(a) (b) (c) (d)

Figure 5. Results for elliptical scatterer, showing gray scale of indicator function, the exact boundary and the estimated boundary for: (a) LSM case; (b) MLSM case; (c) GLSM result with $P = 2$; (d) GLSM result with $P = 3$.

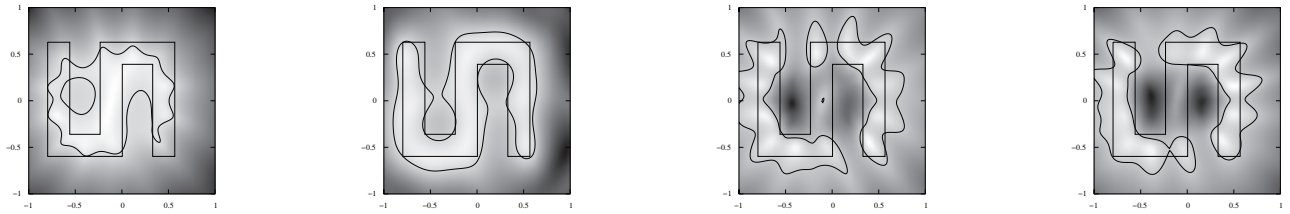

(a) (b) (c) (d)

Figure 6. Results for S-shaped scatterer, showing gray scale of indicator function, the exact boundary and the estimated boundary for: (a) LSM case; (b) MLSM case; (c) GLSM result with $P = 2$; (d) GLSM result with $P = 3$.

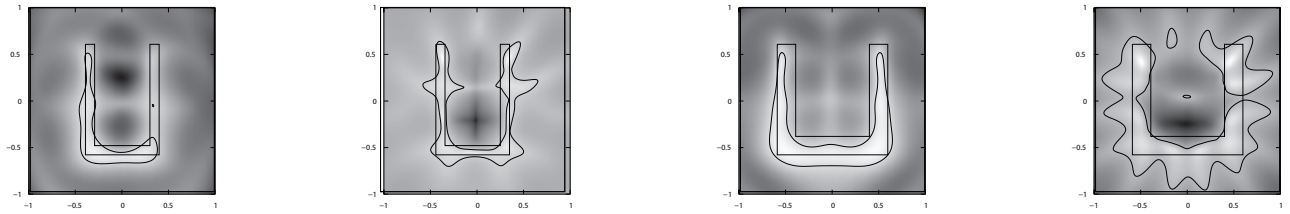

(a) (b) (c) (d)

Figure 7. (a) MLSM results for thin U; (b) GLSM result for thin U with $P = 2$; (c) MLSM boundary estimate for thick U; (d) GLSM result for thick U with $P = 2$.

perform well when the target is very thin (Fig. 7(b)). The MLSM results for the thick target (Fig. 7(c)) are much better than the MLSM results for the thin U shaped scatterer. However, GLSM results for the thick U (Fig. 7(d)) do not improve over what was seen in the previous targets.

The thin U-shaped scatterer has very interesting results. The GLSM result shown in Fig. 7(b) is a much better image compared to the MLSM result in Fig. 7(a). The use of GLSM for very thin features is supported by these results. Thin features may include gaps and/or long thin cracks in objects.

In addition to the visual results provided above, it is also important to consider whether the reconstruction can be obtained without user intervention to improve or optimize the results. For the qualitative methods considered here, the cutoff that determines inside vs. outside the object may require user input to obtain satisfactory results. We now discuss the relative stability of choices of δ. Recall that δ is the number between 0 and 1 that delineates between inside and outside for the indicator functions. Recall I indicates inside when $I > \delta I_{\max}$. See (6), (9), and (13) for the I indicator functions used.

The value of δ for each figure is shown in Table 1 along with the reconstruction technique, either LSM, MLSM, or GLSM2 or GLSM3, depending on P. Examination of the entries in Table 1 shows that the MLSM reconstructions have relatively constant δ at 0.8. This is also suggested in [10]. However, the

Table 1. δ values for Figures 5–7.

Fig. No.	a	b	c	d
5	0.8 (LSM)	0.8 (MLSM)	0.7 (GLSM2)	0.7 (GLSM3)
6	0.8 (LSM)	0.8 (MLSM)	0.65 (GLSM2)	0.65 (GLSM3)
7	0.8 (MLSM)	0.7 (GLSM2)	0.8 (MLSM)	0.55 (GLSM2)

GLSM reconstructions have values of δ in Table 1 that range from 0.55 to 0.7. Therefore, the GLSM reconstruction quality is more reliant on an appropriate choice for δ.

The techniques presented here are not limited to a single object. Multiple objects can be resolved in some cases. As an example of multiple objects, consider the reconstruction of two rods. Results are shown in Fig. 8. One rod is filled ($\epsilon_r = 2$) and one rod is hollow. GLSM requires $\delta = 0.35$ to obtain satisfactory results, shown in Fig. 8(b). The MLSM results using $\delta = 0.8$ are much better, as shown in Fig. 8(a). Clearly, the MLSM method is more robust with respect to inside/outside (i.e., δ) threshold, even for multiple objects.

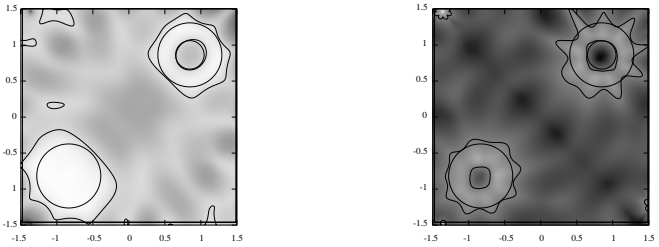

Figure 8. (a) MLSM boundary estimate of two rod object ($\delta = 0.8$); (b) GLSM result using $P = 2$ and $\delta = 0.35$.

4. CONCLUSIONS

In this paper, the LSM method is presented along with two published generalizations. A suitable set of objects was chosen to compare the reconstruction results from each method. Scattered data was computed using MEEP, a FD-TD method. Results indicate that the GLSM method may be more useful in the reconstruction of very thin features. The MLSM method, however, appears to be more practical for the general case and admits a more stable threshold used in the indicator function to obtain consistent results.

REFERENCES

1. Pastorino, M. and A. Randazzo, *Microwave Imaging: Methods and Applications*, Artech House, Boston, MA, 2018.
2. Tobon Vasquez, J. A., R. Scapaticci, G. Turvani, M. Ricci, L. Farina, A. Litman, M. R. Casu, L. Crocco, and F. Vipiana, "Noninvasive inline food inspection via microwave imaging technology: An application example in the food industry," *IEEE Antennas and Propagation Magazine*, Vol. 62, No. 5, 18–32, 2020, doi: 10.1109/MAP.2020.3012898.
3. Neira, L. M., B. D. Van Veen, and S. C. Hagness, "High-resolution microwave breast imaging using a 3-D inverse scattering algorithm with a variable-strength spatial prior constraint," *IEEE Transactions on Antennas and Propagation*, Vol. 65, No. 11, 6002–6014, 2017, doi: 10.1109/TAP.2017.2751668.

4. Hopfer, M., R. Planas, A. Hamidipour, T. Henriksson, and S. Semenov, "Electromagnetic tomography for detection, differentiation, and monitoring of brain stroke: A virtual data and human head phantom study," *IEEE Antennas and Propagation Magazine*, Vol. 59, No. 5, 86–97, 2017, doi: 10.1109/MAP.2017.2732225.
5. Salucci, M., G. Oliveri, A. Randazzo, M. Pastorino, and A. Massa, "Electromagnetic subsurface prospecting by a multifocusing inexact Newton method within the second-order Born approximation," *J. Opt. Soc. Am. A*, Vol. 31, No. 6, 1167–1179, Jun. 2014, doi: 10.1364/JOSAA.31.001167.
6. Palmeri, R., M. T. Bevacqua, A. F. Morabito, and T. Isernia, "Design of artifiial-material-based antennas using inverse scattering techniques," *IEEE Transactions on Antennas and Propagation*, Vol. 66, No. 12, 7076–7090, 2018, doi: 10.1109/TAP.2018.2871707.
7. Bozza, G., M. Brignone, and M. Pastorino, "Aplication of the no-sampling linear sampling method to breast cancer detection," *IEEE Transactions on Biomedical Engineering*, Vol. 57, No. 10, 2525–2534, 2010, doi: 10.1109/TBME.2010.2055059.
8. Catapano, I., F. Soldovieri, and L. Crocco, "On the feasibility of the linear sampling method for 3D GPR surveys," *Progress In Electromagnetics Research*, Vol. 118, 185–203, 2011.
9. Colton, D., H. Haddar, and M. Piana, "The linear sampling method in inverse electromagnetic scattering theory," *Inverse Problems*, Vol. 19, 105–137, 2003.
10. Agarwal, K. and Y. Zhong, "A multipole-expansion based linear sampling method for solving inverse scattering problems," *Optics Express*, Vol. 12, No. 6, 6366–6381, Mar. 2010.
11. Crocco, L., L. Di Donato, I. Catapano, and T. Isernia, "An improved simple method for imaging the shape of complex targets," *IEEE Transactions on Antennas and Propagation*, Vol. 61, No. 2, 843–851, Feb. 2013.
12. Potthast, R., "A study on orthogonality sampling," *Inverse Problems*, Vol. 26, No. 7, 074 015, 2010.
13. Akıncı, M. N., M. Çayören, and İ. Akduman, "Near-field orthogonality sampling method for microwave imaging: Theory and experimental verifiation," *IEEE Trans. Microwave Theory Tech.*, Vol. 64, No. 8, 2489–2501, Aug. 2016.
14. Chen, X., *Computational Methods for Electromagnetic Inverse Scattering*, John Wiley & Sons, Hoboken, NJ, 2018.
15. Bevacqua, M. T. and R. Palmeri, "Qualitative methods for the inverse obstacle problem: A comparison on experimental data," *Journal of Imaging*, Vol. 5, No. 4, 2019, ISSN: 2313-433X, doi: 10.3390/jimaging5040047, [Online]. Available: https://www.mdpi.com/2313-433X/5/4/47.
16. Bevacqua, M. and T. Isernia, "Shape reconstruction via equivalence principles,constrained inverse source problems and sparsity promotion," *Progress In Electromagnetics Research*, Vol. 158, 37–48, 2017.
17. Richmond, J., "Scattering by a dielectric cylinder of arbitrary crossectional shape," *IEEE Transactions on Antennas and Propagation*, Vol. 13, No. 3, 334–341, May 1965.
18. Oskooi, A. F., D. Roundy, M. Ibanescu, P. Bermel, J. D. Joannopoulos, and S. G. Johnson, "MEEP: A flexible free-software package for electromagnetic simulations by the FDTD method," *Computer Physics Communications*, Vol. 181, 687–702, Jan. 2010, doi: doi:10.1016/j.cpc.2009.11.008.
19. Cakoni, F., D. Colton, and P. Monk, "Qualitative methods in inverse electromagnetic scattering theory," *IEEE AP Magazine*, Vol. 59, No. 5, 24–33, Oct. 2017.
20. Catapano, I., L. Crocco, and T. Isernia, "On simple methods for shape reconstruction of unknown scatterers," *IEEE Transactions on Antennas and Propagation*, Vol. 55, No. 5, 1431–1436, May 2007.
21. Crocco, L., I. Catapano, L. Di Donato, and T. Isernia, "The linear sampling method as a way to quantitative inverse scattering," *IEEE Transactions on Antennas and Propagation*, Vol. 60, No. 4, 1844–1853, Apr. 2012.